

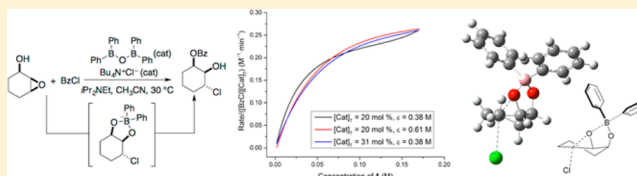
Mechanism of an Organoboron-Catalyzed Domino Reaction: Kinetic and Computational Studies of Borinic Acid-Catalyzed Regioselective Chloroacylation of 2,3-Epoxy Alcohols

Graham E. Garrett,¹ Kashif Tanveer, and Mark S. Taylor^{1*}

Department of Chemistry, University of Toronto, Toronto, Ontario M5S 3H6 Canada

Supporting Information

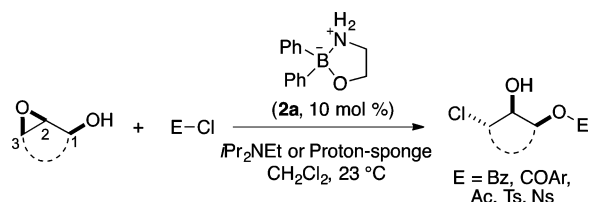
ABSTRACT: A mechanistic study of the borinic acid-catalyzed chloroacylation of 2,3-epoxy alcohols is presented. In this unusual mode of catalysis, the borinic acid activates the substrate toward sequential reactions with a nucleophile (epoxide ring-opening by chloride) and an electrophile (O-acylation of the resulting alkoxide). Reaction progress kinetic analysis of data obtained through in situ FTIR spectroscopy is consistent with a mechanism involving turnover-limiting acylation of a chlorohydrin-derived borinic ester. This proposal is further supported by investigations of the effects of aryl chloride substitution on reaction rate. The kinetics experiments also shed light on the effects of chloride concentration on reaction rate and indicate that the catalyst is subject to inhibition by the product of the chloroacylation reaction. Computational modeling is employed to gain insight into the effects of the organoboron catalyst on the regioselectivities of the epoxide ring-opening and acylation steps. The density functional theory calculations provide a plausible pathway for selective chlorinolysis at C-3 and benzoylation at O-1, as is observed experimentally.



INTRODUCTION

Methods for selective chemical transformations of 2,3-epoxy alcohols are needed to make efficient use of the building blocks generated by diastereo- or enantioselective epoxidations of allylic alcohols.¹ Regioselective ring-opening of 2,3-epoxy alcohols has been a particularly important goal in this regard.² More than two decades ago, Sharpless' group reported that stoichiometric quantities of Ti(OiPr)₄ could be employed to achieve C3-selective opening with diverse nucleophiles.³ Catalytic methods for regioselective ring-opening of epoxy alcohols have emerged more recently, with pioneering results having been achieved by the groups of Yamamoto⁴ and Iwabuchi.⁵ Recently, we reported that 2,3-epoxy alcohols undergo chloroacylation or chlorosulfonylation in the presence of borinic ester 2a (Scheme 1).⁶ The ability to achieve chloride ring-opening and O-functionalization (acylation or sulfonylation) in a single operation was a unique aspect of this catalytic method. It provided a way to differentiate the three contiguous oxygenated positions of the 2,3-epoxy alcohol

Scheme 1. Chloroacylation and Chlorosulfonylation of 2,3-Epoxy Alcohols Catalyzed by 2a



group and was likely important for facilitating catalyst turnover (the previously reported examples of borinic acid-promoted ring-openings of epoxy alcohols have employed stoichiometric quantities of the boron reagent).⁷ This transformation also represented a novel mode of catalytic reactivity for borinic acids, a class of boron compounds that have not been applied extensively in catalysis.^{8,9}

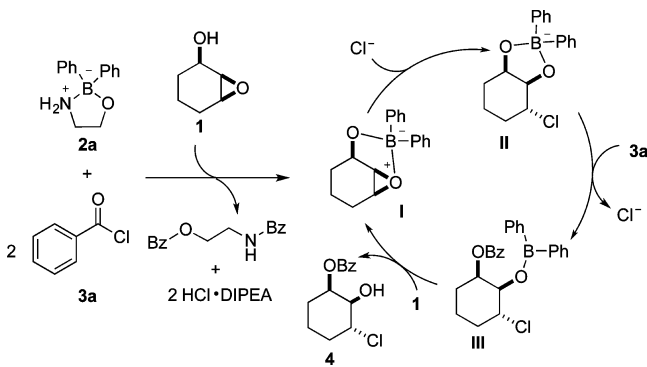
We were motivated to study the mechanism of this transformation for a number of reasons. This type of domino reactivity, wherein a boron catalyst apparently activates the substrate sequentially as an electrophile and a nucleophile, had not been described previously. The kinetics of this process and the origins of regioselectivity in the ring-opening (C3-selective) and O-functionalization (C1-selective) steps were of interest. Furthermore, we have found it challenging to develop analogous processes such as fluoroacylation, azidoacylation, or cyanoacylation of epoxy alcohols. Mechanistic understanding could point toward ways to overcome these limitations. Herein, we describe a study of the mechanism of borinic acid-catalyzed chloroacylation of 2,3-epoxy alcohols using reaction progress kinetic analysis (RPKA)¹⁰ of data obtained using in situ infrared (IR) spectroscopy. Computational modeling with density functional theory (DFT) is used to gain insight into the origins of rate acceleration and regiocontrol for the key borinic acid-catalyzed steps.

Received: November 9, 2016

RESULTS AND DISCUSSION

Proposed Catalytic Cycle. The proposed catalytic cycle for chlorobenzoylation of epoxy alcohol **1** is shown in Scheme 2. Activation of the diphenylborinate precatalyst **2a** via

Scheme 2. Proposed Catalytic Cycle for Chloroacylation of Epoxy Alcohol **1** Using Catalyst **2a**

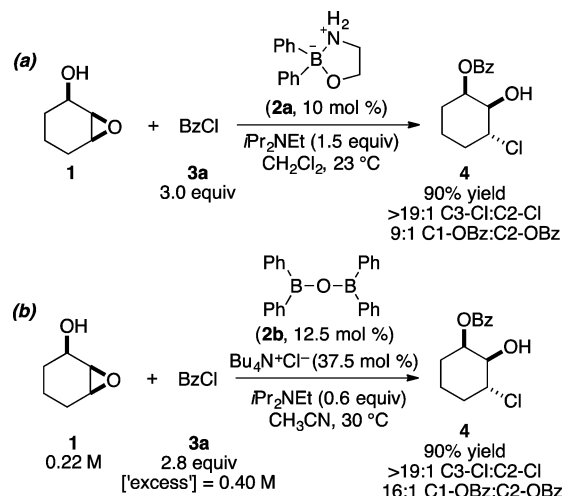


acylation of the ethanolamine ligand releases 2 equiv of chloride relative to the catalyst. The borinic acid then binds reversibly to the 2,3-epoxy alcohol, generating complex **I**. Nucleophilic attack by Cl^- opens the oxirane ring, forming tetra-coordinate boronate intermediate **II**. Acylation of **II** by benzoyl chloride (**3a**) generates complex **III**, which after displacement by the substrate results in catalyst turnover and release of the product (**4**). This proposal was consistent with the following observations from our previous work on borinic acid catalysis and from our initial studies of epoxy alcohol chloroacylation: (1) the epoxy ester derived from **1** did not undergo ring-opening under the reaction conditions, suggesting that ring-opening precedes acylation; (2) both **2a** and related diarylborinic acids activate diols toward regioselective reactions with a variety of electrophiles, including acyl and sulfonyl chlorides;¹¹ (3) N,O-bis-functionalized ethanolamine derivatives have been isolated from diol activation reactions using ethanolamine ester **2a** as precatalyst;¹² and (4) in the absence of catalyst, benzoylation of chlorohydrin diol **5** took place slowly and with low regioselectivity.

Selection of Model System and Reaction Conditions.

The chlorobenzoylation of **1** was selected for mechanistic study due to the ease of preparation of the epoxy alcohol substrate and the high yield and regioselectivity obtained using this combination of reagents under the optimized conditions (90% yield, >19:1 C3:C2, 9:1 O1:O2, Scheme 3a). The reaction conditions were modified to facilitate the acquisition and analysis of rate data. Acetonitrile was employed as the reaction solvent, in place of dichloromethane, both to reduce changes in concentration due to solvent evaporation and to permit analysis of the C–Cl stretching region of the IR spectrum. Reactions were kept at a constant temperature of 30 °C in an oil bath rather than being conducted at ambient temperature. Instead of ethanolamine ester precatalyst **2a**, diphenylborinic anhydride (**2b**) was used in combination with tetrabutylammonium chloride ($\text{Bu}_4\text{N}^+\text{Cl}^-$). Using **2b** and $\text{Bu}_4\text{N}^+\text{Cl}^-$ avoided complications that could arise from slow entry of precatalyst **2a** into the catalytic cycle and permitted independent variation of the concentrations of diphenylborinic acid and chloride. Although **2b** is a dimer in the solid state, it dissociates rapidly to monomers in the presence of alcohols or water. When the **2b**/ $\text{Bu}_4\text{N}^+\text{Cl}^-$ catalyst system was used, the amount of $i\text{Pr}_2\text{NEt}$

Scheme 3. Conditions for Chlorobenzoylation of Epoxy Alcohol **1** (a) as Initially Reported in Ref 6 and (b) as Adapted Here for Acquisition of Reaction Rate Data



could be decreased from 1.5 equiv to 0.6 equiv relative to epoxy alcohol (see below). Product **4** was obtained in high yield and regioselectivity under these modified reaction conditions (Scheme 3b).

Reaction Monitoring and Rate Determinations. The course of a chloroacylation reaction conducted under the conditions shown in Scheme 3b was monitored by ^1H nuclear magnetic resonance (NMR) spectroscopy (Figure 1a). Aliquots were withdrawn at intervals ranging from 3 to 6 min, dried, diluted into CDCl_3 , and analyzed. Clean and complete conversion of the epoxy alcohol to product **4** (along with a small amount of its 2-O-acylated regioisomer) took place over roughly 1 h. Signals corresponding to chlorohydrin diol **5** built up to a maximum within the first 5 min of the reaction and then gradually decreased over the course of the experiment, consistent with the hypothesis that **5** is an intermediate in the pathway leading to product **4**.

To facilitate reaction progress kinetic analysis, the chloroacylation was monitored by in situ FTIR spectroscopy. The appearance of signals at 717 cm^{-1} (the C–Cl bond stretching frequency for product **4** and chlorohydrin diol **5**) and 1278 cm^{-1} (the ester C–O bond stretching frequency for product **4**) was evident as the reaction progressed. The latter signal enabled quantification of product concentration over time, while the former was used to infer the concentration of epoxy alcohol at each time point, based on the assumption that the conversion of **1** is equal to the sum of the concentrations of **4** and **5**. This assumption appears to be justified, given the absence of other intermediates or byproducts as assessed by ^1H NMR spectroscopy, as discussed above. Indeed, the concentrations of **1** and **4** determined by FTIR spectroscopy were in good agreement with the NMR data (Figure 1b). The concentration versus time data from in situ FTIR spectroscopy were fitted to an ordinary differential equation to obtain rate versus time data (see the Experimental Section for details, and the Supporting Information for further discussion). Graphical rate equations of rate versus the concentration of epoxy alcohol **1** for triplicate experiments carried out under the standard conditions showed good overlay, indicating that this protocol provided reproducible kinetic data (Figure 1c).

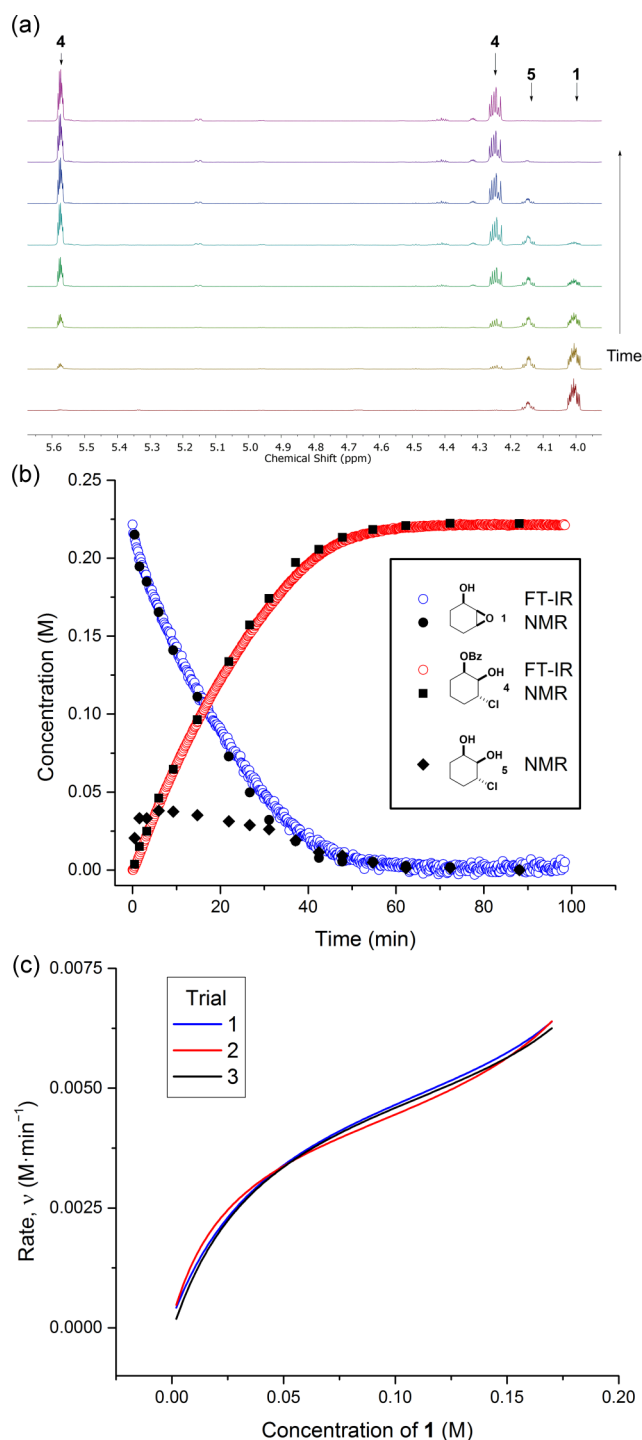


Figure 1. (a) Progress of the chloroacylation reaction of **1** as assessed by ^1H NMR spectroscopy. (b) Concentration versus time data for substrate **1** (as assessed by in situ FTIR (blue \circ) and ^1H NMR spectroscopy (black \bullet)), product **4** (as assessed by in situ FTIR (red \circ) and ^1H NMR spectroscopy (black \blacksquare)) and chlorohydrin **5** (as assessed by ^1H NMR spectroscopy (black \blacklozenge)). (c) Graphical rate equations (rate versus concentration of **1**) for three experiments conducted under the conditions shown in Scheme 3b.

Reaction Progress Kinetic Analysis of Rate Data. The kinetic orders in epoxy alcohol **1**, $(\text{PhB})_2\text{O}$ (**2b**), $\text{Bu}_4\text{N}^+\text{Cl}^-$, BzCl (**3a**), and $i\text{Pr}_2\text{NEt}$ were determined by examining graphical rate equations for reactions conducted at different concentrations of these species. Increases in reaction rate were

observed upon increasing the concentrations of **3a** and **2b**. Normalizing the reaction rates for the total borinic acid concentration and the concentration of BzCl at each point resulted in overlay of the graphical rate eqs (Figure 2a), indicating first-order kinetics in each of these two species. “Different excess” experiments were conducted, and the reaction rate plotted against the concentration of BzCl (Figure 2b). The overlay of graphical rate equations is evident at the initial stages of the reaction points toward pseudo zero-order (saturation) kinetics in **1**. Variation of the concentration of $i\text{Pr}_2\text{NEt}$ showed apparent zero-order kinetics in base (see the Supporting Information).

Considering that the identity of the base was one of the important parameters in the original optimization of the chloroacylation protocol, the observation of zero-order kinetics in base was somewhat surprising. This apparent inconsistency was resolved when we explored the effects of base concentration on reactions conducted under the originally reported protocol, using precatalyst **2a** rather than **2b**/ $\text{Bu}_4\text{N}^+\text{Cl}^-$. Under these conditions, no product formation was observed in the absence of base, and a positive dependence of rate on $i\text{Pr}_2\text{NEt}$ concentration was observed (see the Supporting Information). It appears that the base is needed to neutralize the 2 equiv of HCl generated upon entry of precatalyst **2a** into the cycle, as borinic acid–alcohol binding is favored under basic conditions.¹² We also note that reactions conducted under the standard conditions for kinetic study did not proceed to completion in the absence of base, appearing to “stall” with residual chlorohydrin diol remaining. The origin of this effect is not clear at present.

As mentioned above, the use of the **2b**/ $\text{Bu}_4\text{N}^+\text{Cl}^-$ combination enabled us to vary the amount of chloride while maintaining a constant concentration of the organoboron catalyst (Figure 3a). To analyze the data from experiments of this type, reaction rates at a given epoxide concentration were plotted against $\text{Bu}_4\text{N}^+\text{Cl}^-$ concentration (Figure 3b). At high epoxide concentrations, this is equivalent to comparing initial rates, while at epoxide concentrations ranging from 0.04 to 0.16 M, it is a comparison of steady-state rates. These plots indicate that the rate increases with $\text{Bu}_4\text{N}^+\text{Cl}^-$ concentration up to roughly 60 mM and that saturation kinetics are in effect at higher chloride concentrations. This concentration corresponds to a 1.4:1 ratio of Cl^- to organoboron catalyst, which is lower than the 2:1 ratio that would result from bis-acylation of the ethanolamine ligand when using precatalyst **2a**.

When rate was plotted versus the concentration of **1** for two reactions conducted under “same excess” conditions, overlay of the graphical rate equations was not observed (Figure 4a). This result is consistent with product inhibition or catalyst deactivation. Borinic acids bind relatively tightly to diols in solution,¹³ but their binding to compounds having a single OH group is less favorable. In this case, both the starting 2,3-epoxy alcohol and the product contain only one free hydroxy group, and so they might be expected to show similar affinities for the organoboron catalyst. Indeed, doping the reaction with **4** under the “same excess” conditions produced an overlay in the graphical rate equations and provided better overlap in the offset concentration versus time plots, indicating that the chlorohydrin monoester product inhibits this transformation (Figure 4b).

The kinetic orders determined by the analysis described above are summarized in Figure 5. Taken together, the data suggest that epoxide ring-opening is rapid relative to ester bond

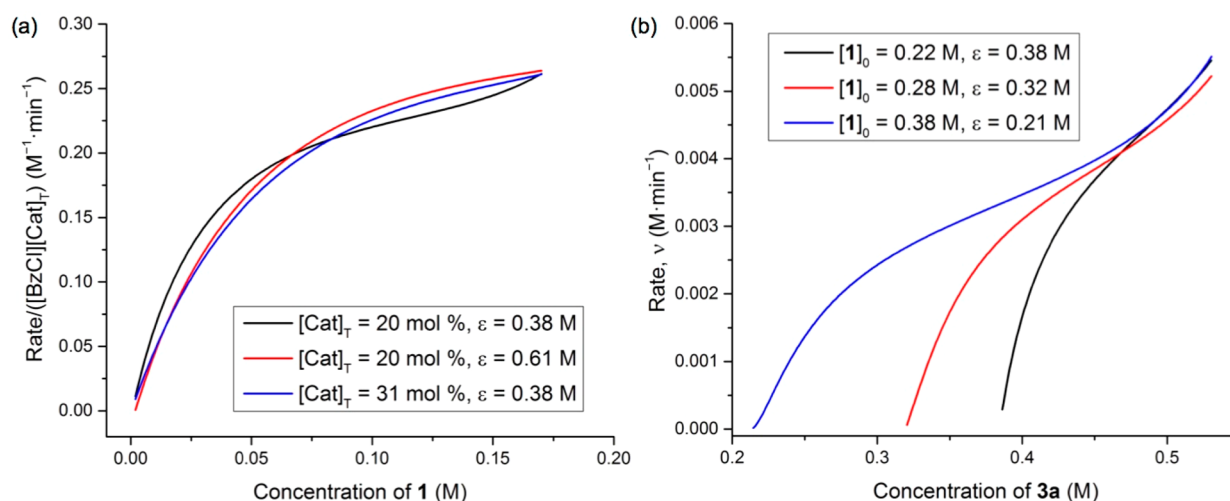


Figure 2. (a) Graphical rate equations (rate versus concentration of **1**) for experiments conducted at different values of the excess ($\epsilon = [\text{BzCl}] - [\text{1}]$) and at different catalyst loadings: $\epsilon = 0.38$ M, 20 mol % catalyst (black —); $\epsilon = 0.61$ M, 20 mol % catalyst (red —); $\epsilon = 0.38$ M, 31 mol % catalyst (blue —). The graphs are normalized for BzCl concentration and catalyst concentration. (b) Graphical rate equations (rate versus concentration of BzCl, **3a**) for “different excess” experiments: $[1]_0 = 0.22$ M, $\epsilon = 0.38$ M (black —); $[1]_0 = 0.28$ M, $\epsilon = 0.32$ M (red —); $[1]_0 = 0.38$ M, $\epsilon = 0.21$ M (blue —).

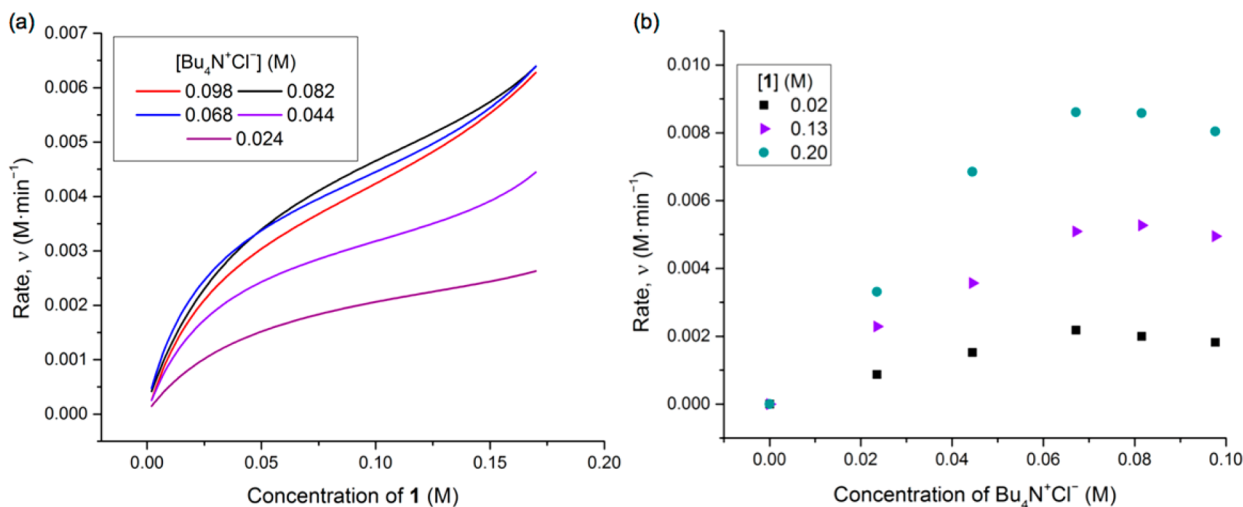


Figure 3. (a) Graphical rate equations for reactions conducted with different loadings of $\text{Bu}_4\text{N}^+\text{Cl}^-$. The $\text{Bu}_4\text{N}^+\text{Cl}^-$ concentrations were 24 mM (purple —), 44 mM (light-purple —), 68 mM (blue —), 82 mM (black —) and 98 mM (red —). (b) Plots of rate versus $\text{Bu}_4\text{N}^+\text{Cl}^-$ loading for epoxy alcohol concentrations of 0.02 M (black ■), 0.13 M (purple triangle) and 0.20 M (teal ●).

formation and that borinic ester **II** is the catalyst resting state. Consistent with this idea, inspection of the IR data from the early stages of the reaction showed an initial period of roughly 30 s in which the absorbance corresponding to C–Cl bond formation increased without evident ester C–O bond formation (see the [Supporting Information](#)). After this initial “burst” of C–Cl bond formation, the C–Cl and C–O FTIR absorption bands were observed to increase at equal rates, presumably indicating that the reaction had reached a steady state. Further support for the assignment of **II** as the catalyst resting state was obtained by in situ monitoring of the chloroacylation reaction by ¹H NMR spectroscopy in CD₃CN (see the [Supporting Information](#)). A new set of signals consistent with structure **II** was observed to build up during the initial stages of the reaction. These signals were distinct from those of “free” chlorohydrin **5**, which was not observed under these conditions. It should be noted that this experiment differs from that described in [Figure 1b](#), in which aliquots of

reaction mixtures were dried and diluted into CDCl₃. For samples treated this way, chlorohydrin **5** was observed rather than complex **II**.

Temperature Dependence of Reaction Rates and Determination of Activation Parameters. Reaction rates were determined at temperatures ranging from 0 to 70 °C. For this set of experiments, the time required for the reaction to reach complete (>95%) conversion ranged from 16 h at 0 °C to 11 min at 70 °C. Plots of $\ln(k/T)$ (where k is the rate constant for the turnover-limiting step, and T is the reaction temperature) versus $1/T$ were generated for epoxy alcohol concentrations within the steady-state regime. A representative plot at $[1] = 0.13$ M is shown in [Figure 6](#). The lines of best fit were used to determine ΔH^\ddagger and ΔS^\ddagger , the enthalpy and entropy of activation, using the Eyring–Polanyi equation. Values of $\Delta H^\ddagger = 13.2 \pm 0.5$ kcal/mol and $\Delta S^\ddagger = -26 \pm 1$ cal/mol·K were obtained using the average values of the slope and intercept of all linear fits within the steady state regime, with

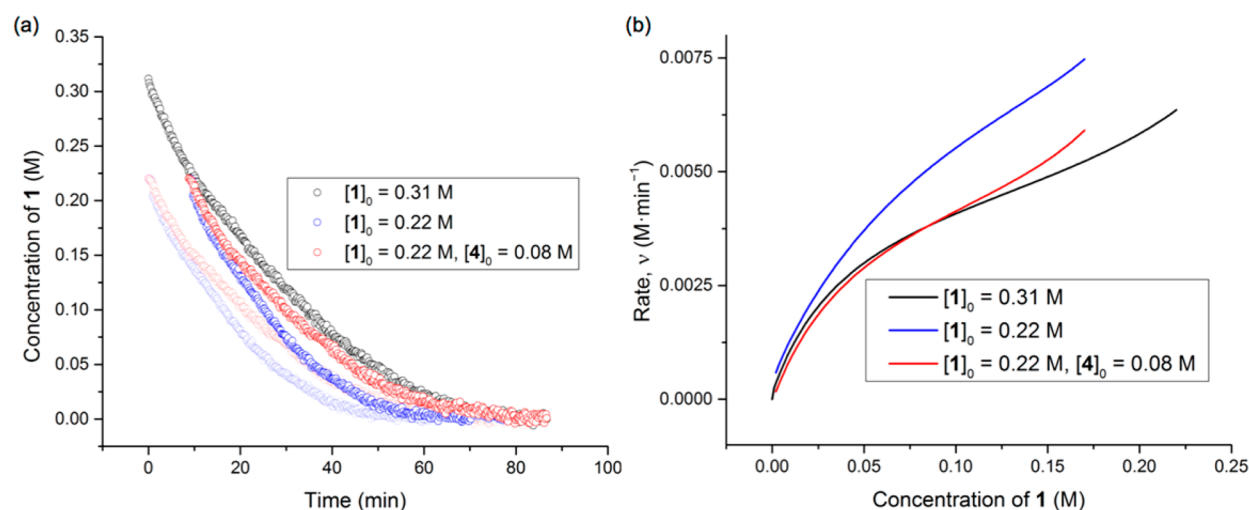


Figure 4. (a) Plots of epoxy alcohol concentration versus time for “same excess” experiments: $[1]_0 = 0.31$ M, $\epsilon = 0.40$ M (black ○), $[1]_0 = 0.22$ M, $\epsilon = 0.40$ M (blue ○), $[1]_0 = 0.22$ M, $\epsilon = 0.40$ M, $[4]_0 = 0.08$ M (red ○). (b) Graphical rate equations corresponding to the “same excess” experiments shown in (a).

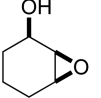
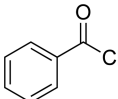
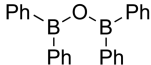
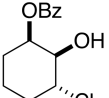
Component	Kinetic order
 1	apparent zero-order (saturation kinetics)
 3a	first-order
<i>i</i> Pr ₂ NEt	zero-order
 2b	first-order
Bu ₄ N ⁺ Cl ⁻	saturation kinetics - first-order at $[Bu_4N^+Cl^-]/[cat]_T < 1.4$ - zero-order at $[Bu_4N^+Cl^-]/[cat]_T > 1.4$
 4	negative order (inhibition)

Figure 5. Summary of kinetic orders determined by reaction progress kinetic analysis.

uncertainties based on the standard deviations of the results. The magnitude of the entropy of activation is consistent with a bimolecular mechanism and appears to be roughly in line with existing data for reactions of acyl chlorides with alcohols (-28 to -34 cal/mol·K).¹⁴

Substituent Effects on Epoxy Alcohol Chloroacylation. Chloroacylations of **1** were conducted using 4-methoxybenzoyl chloride (**3b**) and 4-nitrobenzoyl chloride (**3c**) to assess the effects of aroyl chloride substitution on reaction rate. Consistent with acylation being the turnover-limiting step of the reaction, the chloroacylation rates increased in the order **3b** < **3a** < **3c**: the reaction of the electron-rich methoxy-substituted derivative required 5 h to reach completion, whereas that of the nitro-substituted derivative

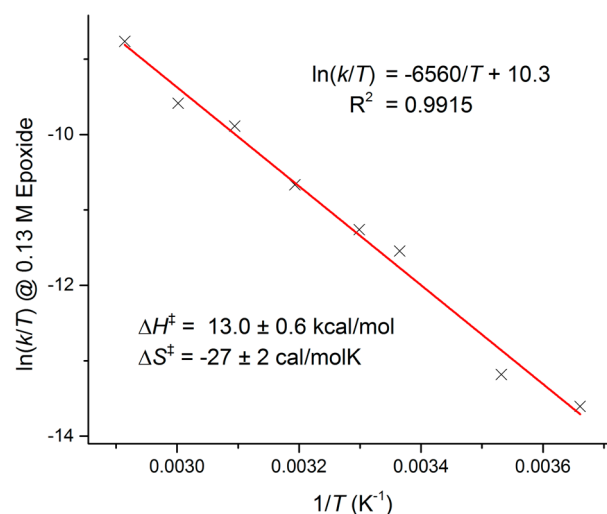


Figure 6. Plot of $\ln(k/T)$ vs $1/T$ (where k is the second-order rate constant for the turnover-limiting step, calculated at $[1] = 0.13$ M, and T is the reaction temperature) for temperatures ranging from 0 to 70 °C.

was complete in roughly 7 min (Figure 7a). Contrary to the results discussed above for the reaction of benzoyl chloride, changing the “excess” of **3c** had no effect on the rate of the reaction (Figure 7b). The reaction of 4-nitrobenzoyl chloride thus shows zero-order kinetics in acylating agent and first-order kinetics in epoxy alcohol (as inferred from the linear dependence of rate on $[1]$ in the graphical rate eq (Figure 7b, inset)). This rate law is consistent with a change in the turnover-limiting step from acylation to epoxide ring-opening when the more reactive electrophile is employed.

Chlorohydrin Diol Complex As a Reactive Intermediate. The NMR reaction monitoring experiments discussed above (Figure S7) suggested that chlorohydrin diol complex **II** was a reactive intermediate in the chloroacylation of **1**. Compound **5**, a precursor to this complex, was synthesized by the ring-opening of **1** with lithium chloride in the presence of acetic acid and trimethyl borate^{7b} and subjected to benzoyl chloride in the presence of catalyst **2b**. Unlike the chloroacylation of **1**, this reaction generates HCl as a

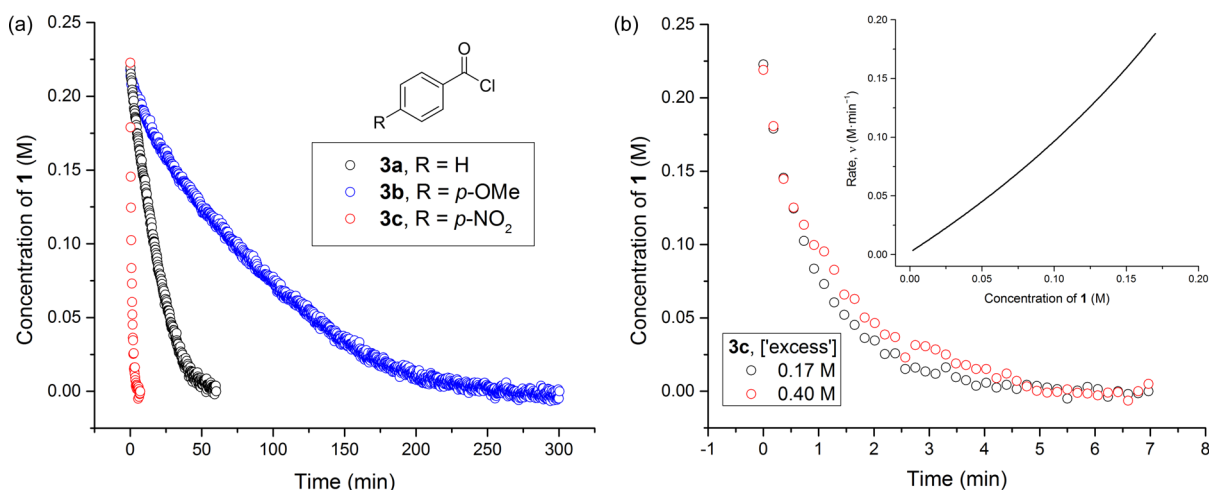


Figure 7. (a) Plots of epoxy alcohol concentration versus time for experiments using substituted aryl chlorides **3a** (black O), **3b** (blue O) and **3c** (red O). (b) Plots of epoxy alcohol versus time for “different excess” experiments using 4-nitrobenzoyl chloride (**3c**): $\epsilon = 0.17$ M (black O) and $\epsilon = 0.40$ M (red O); inset: graphical rate equation for the reaction of **1** with **3c** ($\epsilon = 0.17$ M).

byproduct, and so 1.7 equiv of *i*Pr₂NEt was added. Reaction progress was assessed using the appearance of the ester C–O stretch in the FTIR spectrum to determine the concentration of product. The rate of this reaction was roughly similar to that of BzCl with epoxy alcohol **1** (Figure 8), although differences in

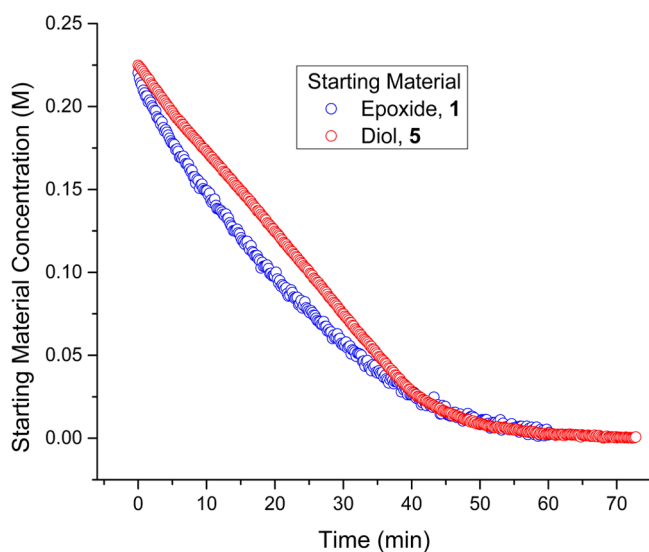


Figure 8. Plots of substrate concentration versus time for reactions of BzCl ($\epsilon = 0.40$ M) with epoxy alcohol **1** (blue O) and chloridiol **5** (red O).

the concentration versus time profiles were evident. Exact overlay of the concentration versus time curves would not be expected, given that the reactions are not identical and occur under different conditions. For example, product inhibition was implicated for the chloroacylation of **1**, but is unlikely to be significant for the benzylation of diol **5**. Nonetheless, the fact that the reactions of **1** and **5** follow roughly similar time courses is in keeping with acylation being the rate-determining step of the epoxy alcohol chloroacylation process.

Computational Modeling. The proposed reaction pathway was modeled using DFT calculations. The effects of the borinic acid catalyst on the regiochemical outcome of the epoxide opening and O-acylation steps were of particular

interest, since this type of information could not be inferred from our studies of the reaction rates. The B3LYP DFT functional and 6-31+G(d,p) basis set were employed for these calculations. This level of theory was selected due to its low computational overhead and ease of handling large molecules, and to enable comparisons with previous computational studies of 2,3-epoxy alcohol ring-opening reactions.^{7a,15}

We began by modeling the borinic acid-catalyzed ring-opening step (Figure 9). The lowest-energy calculated structures of the epoxy alcohol-derived diphenylborinic ester (of which the most stable places the –OBPh₂ substituent in the pseudoequatorial position of the half-chair) showed only single-point binding to the boron center. In contrast, previous computational studies pointed toward chelation of the hydroxy and epoxide oxygens in analogous complexes of epoxy alcohols with phenylboronic acid⁷ or lithium cation.¹⁵ However, an interaction between boron and the developing alkoxide was evident in the calculated transition state for the ring-opening step. Attack of chloride at C-3 occurs through a boatlike transition state, accessed via a higher-energy borinic ester conformer in which the –OBPh₂ substituent is pseudoaxial (Figure 10). A pathway for chloride attack at C-2 was also found, proceeding through a twist-chairlike transition-state structure. This latter transition state was 4.0 kcal/mol higher in energy than that of the boatlike transition state for attack at C-3, consistent with the high level of C3-selectivity obtained in the borinic acid-catalyzed reaction.

An analogous set of calculations was carried out for the uncatalyzed epoxide ring-opening (Figures 9 and 10). The lowest-energy uncatalyzed pathway involves attack at C-2 through a chairlike transition state, leading to a product conformer having chloro and alkoxide groups in axial positions in accordance with the Füst–Plattner rule.¹⁶ Another chairlike transition state leading to attack at C-3 was found to be only marginally higher in energy (+1.1 kcal/mol). The lower-energy of the two transition states arises from the half-chair conformer in which the OH group occupies a pseudoaxial position and is thus able to stabilize the developing negative charge through hydrogen bonding. While experimental data that can be compared directly to these calculations do not exist, the results are consistent with previous studies showing that mixtures of products are formed upon ring-opening of epoxy alcohols in

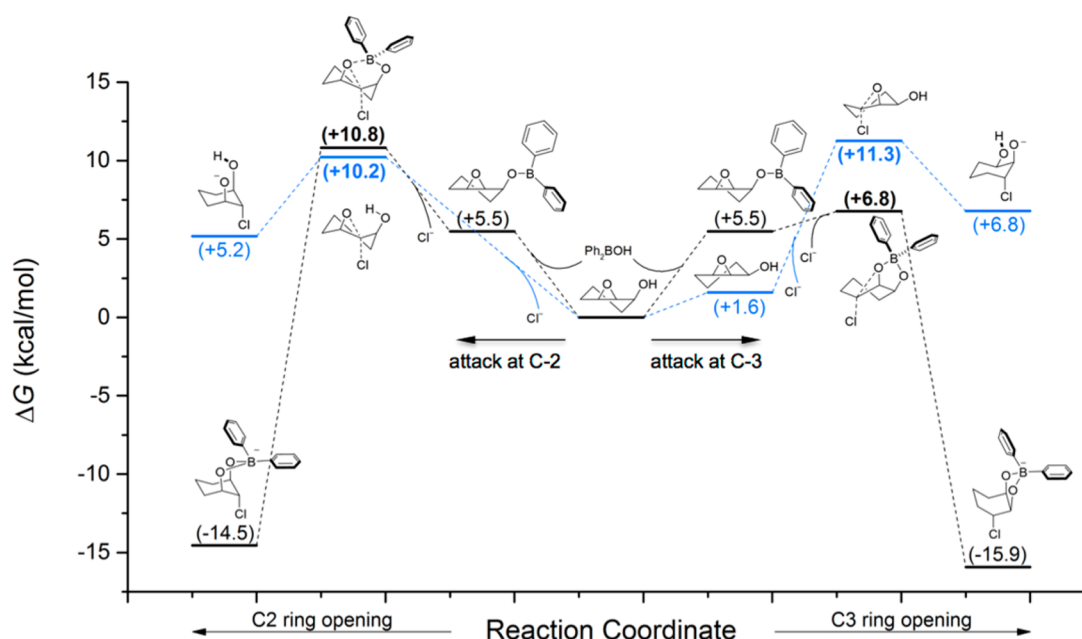
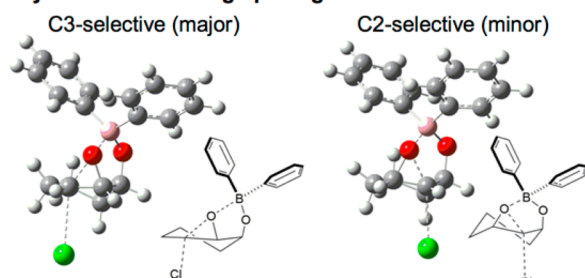


Figure 9. Potential energy surfaces for borinic acid-catalyzed (black —) and uncatalyzed (blue —) chlorinolysis of epoxy alcohol **1**, calculated at the B3LYP/6-31+G(d,p) level of theory. Pathways leading to ring-opening at C-2 (arrow pointing to the left) and C-3 (arrow pointing to the right) are shown.

Catalyst-accelerated ring opening:



Uncatalyzed ring opening:

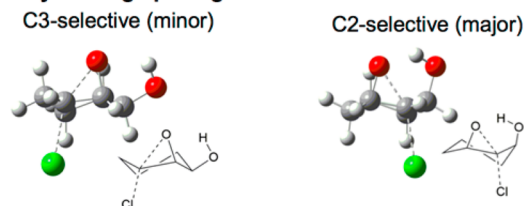


Figure 10. Transition-state structures for: borinic acid-catalyzed ring-opening of **1** at C-3; borinic acid-catalyzed ring-opening of **1** at C-2; uncatalyzed ring-opening of **1** at C-3; and uncatalyzed ring-opening of **1** at C-2, calculated at the B3LYP/6-31+G(d,p) level of theory.

the absence of Lewis acid additives.¹⁷ They indicate that the borinic acid catalyst has a significant effect on the regiochemical outcome of the epoxide chlorinolysis step.

We then turned our attention to the benzoylation step (Figure 11). The tetracoordinate borinate formed by attack of chloride at C-3 can undergo relaxation from the boat conformation to two lower-energy chairlike conformers, with the most stable (by 0.7 kcal/mol) having the chlorine substituent in an equatorial position. However, the lowest-energy benzoylation pathway was found to proceed from the chairlike conformer having the axial chloro group. In this conformation, it is the equatorial oxygen that undergoes functionalization, in agreement with the selectivity pattern for

borinic acid-catalyzed reactions of pyranoside derivatives.^{11a} The transition state leading to the 2-O-benzoylated product was 3.1 kcal/mol higher in energy, consistent with the high regioselectivity that was observed experimentally. Benzoylation was calculated to take place through an S_N2 -type mechanism, in which C–O bond formation and C–Cl bond cleavage occur in a concerted fashion through a tetrahedral transition state (Figure 12). Numerous alternative computational approaches were explored, including *ab initio* HF and MP2 methods as well as the M06-2X, B97D3, and B2PLYP DFT functionals, but in no case could a tetrahedral intermediate of the type expected from an addition–elimination pathway be identified as an energy minimum. The question of concerted versus addition–elimination mechanisms for the benzoylation step is not the primary focus of this work, but we note that several prior computational studies have identified the S_N2 -type mechanism as a viable pathway for nucleophilic substitutions of acyl chlorides^{18,19} and that experimental evidence consistent with a concerted, bimolecular mechanism has also been obtained²⁰ for solvolysis^{21,22} and gas-phase acyl transfer reactions.²³ This observation does not appear to be a unique feature of the borinic acid-catalyzed acylation, as we were also unable to locate tetrahedral intermediates as energy minima for the reactions of the corresponding free alkoxides with BzCl (data not shown).

The overall calculated reaction pathway for chloroacylation is depicted in Figure 13. Quantitative agreement between the gas-phase calculations and the experimental data would not be expected, but to the extent that the calculations indicate that the chlorohydrin-derived borinic ester is the resting state of the catalyst and that benzoylation is turnover-limiting, the results are qualitatively consistent with the experimentally determined kinetic orders. The calculated energies of complexation of Ph₂BOH (used as a proxy for the (Ph₂B)₂O precatalyst that was employed in the experiments) with substrate **1** and product **4** were +5.5 kcal/mol and +6.4 kcal/mol, respectively. That these energies are within 1 kcal/mol of each other is compatible with

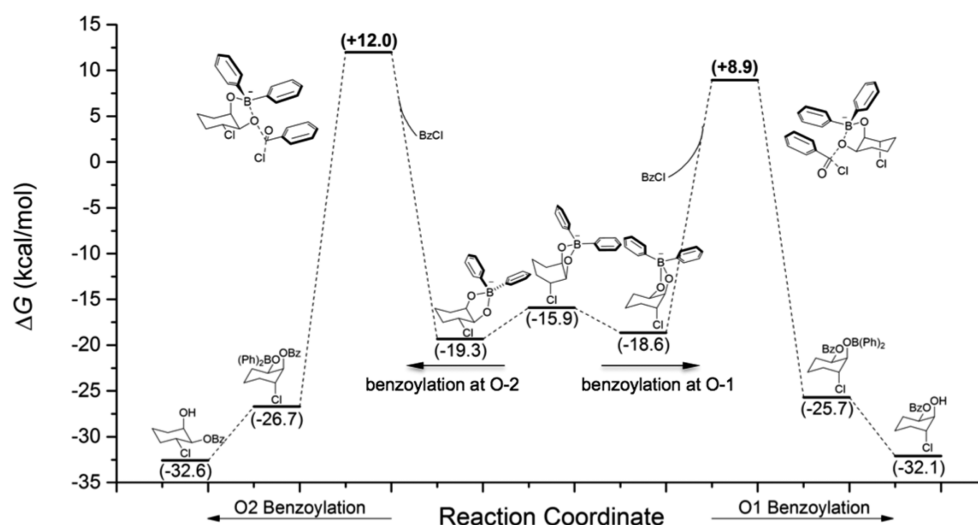


Figure 11. Potential energy surface for benzoylation of borinic ester **II**, calculated at the B3LYP/6-31+G(d,p) level of theory. Pathways leading to benzoylation at O-2 (arrow pointing to the left) and O-1 (arrow pointing to the right) are shown.

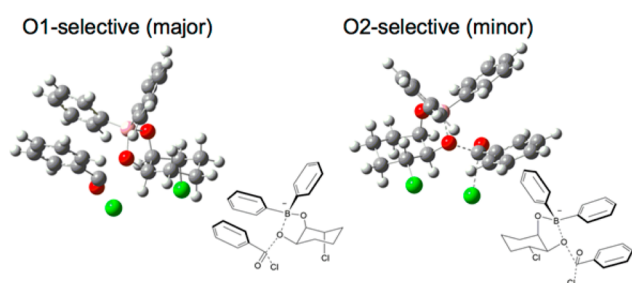


Figure 12. Transition-state structures for benzoylation of **II** at O-1 (major product) and O-2 (minor product), calculated at the B3LYP/6-31+G(d,p) level of theory.

the product inhibition inferred from the “same excess” experiments (Figure 4).

CONCLUSIONS

The kinetics experiments and computational modeling that we have carried out have solidified the mechanistic proposal depicted in Scheme 2 and have deepened our understanding of

the borinic acid-catalyzed chloroacylation process in several important ways. The experimental kinetic orders and the effects of aroyl chloride substitution on reaction rate indicate that the acylation step is turnover limiting. Thus, even at the relatively low chloride ion concentrations resulting from entry of the ethanolamine ester precatalyst into the cycle via reaction of the ligand with BzCl, epoxide ring-opening is fast in comparison to the reaction of the formed borinic ester with BzCl. However, if a sufficiently reactive acylating agent is used (e.g., 4-nitrobenzoyl chloride), epoxide ring-opening becomes turnover-limiting. The primary role of the base is to neutralize the acid generated in the precatalyst activation step, and the reaction shows overall zero-order dependence on base concentration. The calculations reveal an important role for the borinic acid in the ring-opening step, both in providing rate acceleration and in favoring attack of chloride at C-3 through a boatlike transition state. Turnover-limiting acylation apparently proceeds from a borinic ester conformer in which the chloro group occupies an axial position. This pathway may allow for a sterically favorable approach of the electrophile to the position that is not deactivated by the inductive electron-withdrawing effect of the

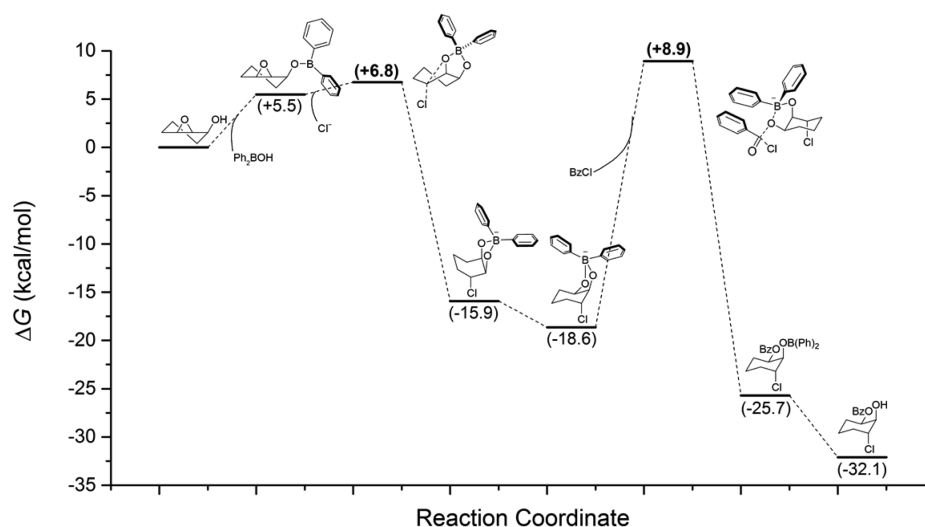


Figure 13. Potential energy surface for borinic acid-catalyzed chloroacylation of **1**, calculated at the B3LYP/6-31G+(d,p) level of theory.

chloro substituent. The “same excess” kinetics experiments reveal an appreciable level of product inhibition, a phenomenon we have not encountered in borinic acid-catalyzed reactions of diols. The computational results also point toward product inhibition, as they show that both substrate and product interact with the catalyst through single-point binding and with similar affinities. The relatively low affinity of the catalyst for the epoxy alcohol may be one of the issues to be addressed if this type of reactivity is to be expanded to other substrate classes. Given the numerous types of functionalized and stereochemically defined products that can be accessed from epoxy alcohols and related substrates, such expansions are worthy of further study.

■ EXPERIMENTAL SECTION

General. Commercially available reagents were used as received with the following exception: acetonitrile was purified by being passed through columns of activated alumina under argon and then degassed for 25 min by sparging with argon. Stainless steel needles and gastight syringes were used to transfer all liquids. Deionized water was obtained from an in-house supply. NMR spectra were obtained on a 500 MHz instrument equipped with a 5 mm cryogenically cooled probe or a 5 mm H/F{X} probe. Chemical shifts δ are reported in ppm relative to tetramethylsilane, referenced to residual protium in the solvent. Spectral features are reported in the following order: chemical shift (δ , ppm); multiplicity (s, singlet; d, doublet; t, triplet; q, quartet; m, complex multiplet; br, broad); number of protons; coupling constants (J , Hz). High-resolution mass spectra (HMRS) were obtained using a time-of-flight mass spectrometer equipped with a direct analysis in real time (DART) ion source.

Substrate and Catalyst Preparation. (\pm)-7-Oxabicyclo[4.1.0]heptan-2-ol (**1**) was prepared according to a previously reported protocol.⁶ NMR spectra were consistent with previously reported data.²⁴ ¹H NMR (500 MHz, chloroform-*d*) δ 3.99 (dddd, J = 9.0, 7.9, 4.9, 2.9 Hz, 1H), 3.33 (m, 1H), 3.30 (m, 1H), 2.13 (d, J = 8.9 Hz, 1H), 1.90–1.81 (m, 1H), 1.81–1.72 (m, 1H), 1.61–1.49 (m, 2H), 1.49–1.38 (m, 1H), 1.31–1.19 ppm (m, 1H). ¹³C NMR (126 MHz, chloroform-*d*) δ 67.2, 55.6, 55.5, 29.1, 23.2, 18.3 ppm.

1,1,3,3-Tetraphenyldiboroxane (**2b**) was prepared by hydrolysis of 2-aminoethyl diphenylborinate (**2a**). Compound **2a** (732.5 mg, 3.25 mmol) was suspended in 4.2 mL of a 50/50 methanol/acetone solution and placed in an ice bath to cool to 0 °C. To this was added 4.2 mL of 1 M HCl(aq), and the mixture stirred at 0 °C. After 40 min, the reaction was diluted with 4 mL of water and then extracted three times with 4 mL of diethyl ether. The organics were then pooled and washed twice with 4 mL of water and once with 4 mL of brine. The organics were then dried over magnesium sulfate, filtered, and concentrated in vacuo without heating. The material was dried further under high vacuum until a white solid resulted. 1,1,3,3-Tetraphenyldiboroxane (**2b**) was obtained as a white solid (419.2 mg, 1.21 mmol, 75% yield). The ¹H NMR spectrum (DMSO-*d*₆ with a drop of D₂O) was consistent with the reported data for Ph₂BOH.²⁵ The solid was stored at 0 °C in a glovebox under nitrogen. ¹H NMR (500 MHz, DMSO-*d*₆) δ 7.64–7.59 (m, 4H), 7.45–7.40 (m, 2H), 7.39–7.34 ppm (m, 4H). ¹³C NMR (126 MHz, DMSO-*d*₆) δ 139.0, 135.6, 131.7, 129.0 ppm.

(1*R**,2*R**,3*R**)-(\pm)-3-Chlorocyclohexane-1,2-diol (**5**). Prepared according to a previously reported protocol.^{7b,6} NMR

spectra were consistent with previously reported data.⁶ ¹H NMR (500 MHz, chloroform-*d*) δ 4.19–4.10 (m, 2H), 3.55 (app dt, J = 9.3, 2.3 Hz, 1H), 2.71 (s, 1H), 2.35 (s, 1H), 2.21 (dddd, J = 11.2, 5.5, 4.4, 2.8 Hz, 1H), 1.98–1.89 (m, 1H), 1.82–1.68 (m, 1H), 1.69–1.61 (m, 1H), 1.60–1.45 ppm (m, 2H). ¹³C NMR (126 MHz, chloroform-*d*) δ 105.2, 69.4, 62.9, 34.4, 30.0, 19.7 ppm.

Reaction Monitoring Protocol and Data Analysis.

(\pm)-7-Oxabicyclo[4.1.0]heptan-2-ol (**1**) (17.7 mg, 0.16 mmol) was weighed into a two-neck conical flask equipped with a magnetic stir bar. A 6.35 mm attenuated total reflection (ATR) probe with diamond sensor, connected by fiber optic cable to a mid-infrared FTIR spectrometer, was used for reaction monitoring. The probe was inserted into the flask, and the second neck sealed with a fresh septum. The flask was then purged with argon for 15 min and then 235 μ L of acetonitrile was added to the flask. The vessel was submerged into an oil bath set to 30 °C with the stir rate set to 250 rpm. *N,N*-Diisopropylethylamine (*i*Pr₂NEt) (15 μ L, 11.1 mg, 0.09 mmol) was added to the flask and allowed to stir. Weighed into a 1/2-dram vial in the glovebox, 1,1,3,3-tetraphenyldiboroxane (**2b**) (6.6 mg, 0.02 mmol) and tetra-*n*-butylammonium chloride (Bu₄N⁺Cl[−]) (14.4 mg, 0.06 mmol) were dissolved in 500 μ L of acetonitrile with sonication and light heating. Benzoyl chloride (**3a**) (50 μ L, 57.9 mg, 0.41 mmol) was then injected into the flask, followed immediately by 400 μ L of the acetonitrile solution of **2b** and Bu₄N⁺Cl[−]. The total volume for the reaction was 700 μ L. Spectra were acquired at roughly 15-s intervals, and the reaction conducted under these conditions required roughly 60 min to reach completion. The appearance of the signal at 1278 cm^{−1} (ester C–O stretch) was used to determine the concentration of product. The concentration of starting material was determined indirectly, by taking the difference between the initial epoxy alcohol concentration and the total concentration of chlorine-containing products inferred from the absorbance at 717 cm^{−1} (C–Cl stretch). The concentration vs time data were then fitted to the ordinary differential equation in eq 1, where *a*, *b*, *c*, *d*, *e*, and *f* are fitted parameters and [**1**] is calculated from the difference between the initial epoxide concentration and the amount of C–Cl bond formation. A full discussion of the derivation and validation of the fitting methodology is provided as Supporting Information.

$$\frac{d[\mathbf{1}]}{dt} = \frac{a[\mathbf{1}] + b[\mathbf{1}]^2 + c[\mathbf{1}]^3}{1 + d[\mathbf{1}] + e[\mathbf{1}]^2 + f[\mathbf{1}]^3} \quad (1)$$

After fitting, inputting [**1**] into eq 1 produced the graphical rate equations used in this study.

Reaction Products. (1*R**,2*R**,3*R**)-(\pm)-3-Chloro-2-hydroxycyclohexyl benzoate (**4**) was isolated from a reaction conducted according to the monitoring protocol described above (0.16 mmol scale). Analysis of the unpurified reaction mixture by ¹H NMR spectroscopy showed a 16:1 ratio (1-OBz:2-OBz) of benzoylated regioisomers. Solvent was removed in vacuo, and the residue was purified by flash chromatography on silica gel, eluting with hexanes/ethyl acetate (gradient elution, 100/0 \rightarrow 80/20). The product was obtained as a white solid (28.1 mg, 0.11 mmol, 71% yield). The ¹H NMR spectrum (DMSO-*d*₆) was consistent with the reported data.⁶

(1*R**,2*R**,3*R**)-(\pm)-3-Chloro-2-hydroxycyclohexyl 4-nitrobenzoate was isolated from a reaction conducted according to the monitoring protocol described above (0.16 mmol scale), using 4-nitrobenzoyl chloride as the electrophile. Analysis of

the unpurified reaction mixture by ^1H NMR spectroscopy showed a 9.3:1 ratio (1-OCOAr:2-OCOAr) of acylated regioisomers. Solvent was removed in vacuo, and the residue was purified by flash chromatography on silica gel, eluting with hexanes/ethyl acetate (gradient elution, 100/0 \rightarrow 80/20). The product was obtained as a white solid. ^1H NMR (500 MHz, chloroform-*d*) δ 8.31–8.27 (m, 2H), 8.22–8.18 (m, 2H), 5.64–5.60 (m, 1H), 4.26–4.19 (m, 1H), 3.84 (app dt, J = 9.1, 3.0 Hz, 1H), 2.58 (d, J = 3.2 Hz, 1H), 2.39–2.29 (m, 1H), 2.15–2.04 (m, 1H), 1.87–1.64 ppm (m, 4H). ^{13}C NMR (126 MHz, chloroform-*d*) δ 164.1, 150.8, 135.7, 130.9, 123.7, 75.0, 73.6, 62.0, 33.7, 28.3, 20.2 ppm.

The minor regioisomer ((1*R**,2*R**,6*R**)-(\pm)-2-chloro-6-hydroxycyclohexyl 4-nitrobenzoate) was obtained as a white solid. ^1H NMR (500 MHz, chloroform-*d*) δ 8.35–8.29 (m, 2H), 8.29–8.24 (m, 2H), 5.17 (dd, J = 9.2, 2.8 Hz, 1H), 4.43 (app td, J = 9.8, 4.5 Hz, 1H), 4.36 (dd, J = 5.3, 2.7 Hz, 1H), 2.35–2.26 (m, 1H), 2.00–1.91 (m, 1H), 1.87–1.77 (m, 3H), 1.77–1.66 ppm (m, 2H). ^{13}C NMR (126 MHz, chloroform-*d*) δ 164.0, 150.9, 135.2, 131.1, 123.8, 79.4, 68.5, 57.2, 30.5, 19.2 ppm.

(1*R**,2*R**,3*R**)-(\pm)-3-Chloro-2-hydroxycyclohexyl 4-methoxybenzoate was isolated from a reaction conducted according to the monitoring protocol described above (0.16 mmol scale), using 4-methoxybenzoyl chloride as the electrophile. Analysis of the unpurified reaction mixture by ^1H NMR spectroscopy showed a 11:1 ratio (1-OCOAr:2-OCOAr) of acylated regioisomers. Solvent was removed in vacuo, and the residue was purified by flash chromatography on silica gel, eluting with hexanes/ethyl acetate (gradient elution, 100/0 \rightarrow 80/20). The product was obtained as a white solid (6.5 mg, 0.02 mmol, 15% yield). Difficulties in separating the two regioisomers resulted in a relatively low isolated yield. ^1H NMR (500 MHz, chloroform-*d*) δ 7.98 (app d, J = 9.0 Hz, 2H), 6.92 (app d, J = 9.0 Hz, 2H), 5.54 (app dt, J = 5.0, 2.6 Hz, 1H), 4.23 (ddd, J = 9.9, 8.9, 4.4 Hz, 1H), 3.86 (s, 3H), 3.80 (dd, J = 9.0, 3.0 Hz, 1H), 2.35–2.26 (m, 1H), 2.11–2.01 (m, 1H), 1.80–1.61 ppm (m, 4H). ^{13}C NMR (126 MHz, chloroform-*d*) δ 165.8, 163.7, 131.8, 122.6, 113.8, 75.2, 72.4, 62.1, 55.6, 33.9, 28.4, 20.2 ppm. HRMS (DART, m/z): calculated for $\text{C}_{14}\text{H}_{17}\text{ClO}_4$ ($[\text{M} + \text{H}]^+$): 285.08936, found: 285.08954.

The minor regioisomer ((1*R**,2*R**,6*R**)-(\pm)-2-chloro-6-hydroxycyclohexyl 4-methoxybenzoate) was obtained as an oil (0.8 mg, 0.003 mmol, 2% yield). ^1H NMR (500 MHz, chloroform-*d*) δ 8.04 (app d, J = 9.0 Hz, 2H), 6.95 (app d, J = 9.0 Hz, 2H), 5.13 (dd, J = 8.9, 2.8 Hz, 1H), 4.43–4.36 (m, 1H), 4.31 (app dt, J = 5.6, 2.8 Hz, 1H), 2.27 (dt, J = 12.0, 4.4 Hz, 1H), 1.98–1.86 (m, 1H), 1.86–1.62 ppm (m, 4H). ^{13}C NMR (chloroform-*d*) δ 165.5, 163.9, 132.0, 122.1, 113.9, 77.9, 68.6, 57.5, 55.6, 30.3, 29.9, 19.3 ppm.

Computational Methods. DFT calculations were carried out using the Gaussian 09 suite of programs²⁶ at the B3LYP/6-31+G(d,p) level of theory.²⁷ Vibrational frequency calculations were carried out for each stationary point to ensure they were either an energy minimum (no imaginary frequencies) or a transition state (one imaginary frequency) on the potential energy surface. All transition-state trajectories were confirmed using the intrinsic reaction coordinate method. All frequency calculations were carried out at 1 atm and 298.15 K. Structures were visualized using GaussView 5.0.

■ ASSOCIATED CONTENT

Supporting Information

The Supporting Information is available free of charge on the ACS Publications website at DOI: 10.1021/acs.joc.6b02702.

Kinetic data and analysis methodology, copies of ^1H and ^{13}C NMR spectra, coordinates and energies for calculated structures (PDF)

■ AUTHOR INFORMATION

Corresponding Author

*E-mail: mtaylor@chem.utoronto.ca.

ORCID

Graham E. Garrett: 0000-0001-8558-2027

Mark S. Taylor: 0000-0003-3424-4380

Notes

The authors declare no competing financial interest.

■ ACKNOWLEDGMENTS

This work was supported by NSERC (Discovery Grants and Canada Research Chairs programs), the Canada Foundation for Innovation (Project nos. 17545 and 19119), the Province of Ontario, and by fellowships to G.E.G. (NSERC and the Province of Ontario). The DFT calculations were carried out at the Centre for Advanced Computing (<http://cac.queensu.ca>).

■ REFERENCES

- (1) (a) Katsuki, T.; Martin, V. Asymmetric Epoxidation of Allylic Alcohols: the Katsuki–Sharpless Epoxidation Reaction. In *Organic Reactions*; John Wiley & Sons, Inc.: Hoboken, NJ, 2004. (b) Katsuki, T.; Sharpless, K. B. *J. Am. Chem. Soc.* **1980**, *102*, 5974–5976.
- (2) (a) Hanson, R. M. *Chem. Rev.* **1991**, *91*, 437–475. (b) Pena, P. C. A.; Roberts, S. M. *Curr. Org. Chem.* **2003**, *7*, 555–571. (c) Ko, S. Y.; Sharpless, K. B. *J. Org. Chem.* **1986**, *51*, 5413–5415.
- (3) Caron, M.; Sharpless, K. B. *J. Org. Chem.* **1985**, *50*, 1557–1560.
- (4) (a) Wang, C.; Yamamoto, H. *J. Am. Chem. Soc.* **2014**, *136*, 6888–6891. (b) Wang, C.; Yamamoto, H. *Org. Lett.* **2014**, *16*, 5937–5939. (c) Wang, C.; Yamamoto, H. *Angew. Chem., Int. Ed.* **2014**, *53*, 13920–13923. (d) Wang, C.; Luo, L.; Yamamoto, H. *Acc. Chem. Res.* **2016**, *49*, 193–204.
- (5) Uesugi, S.-i.; Watanabe, T.; Imaizumi, T.; Shibuya, M.; Kanoh, N.; Iwabuchi, Y. *Org. Lett.* **2014**, *16*, 4408–4411.
- (6) Tanveer, K.; Jarrah, K.; Taylor, M. S. *Org. Lett.* **2015**, *17*, 3482–3485.
- (7) (a) Sasaki, M.; Tanino, K.; Hirai, A.; Miyashita, M. *Org. Lett.* **2003**, *5*, 1789–1791. (b) Tomata, Y.; Sasaki, M.; Tanino, K.; Miyashita, M. *Tetrahedron Lett.* **2003**, *44*, 8975–8977.
- (8) (a) Ishihara, K.; Kurihara, H.; Yamamoto, H. *Synlett* **1997**, 1997, 597–599. (b) Ishihara, K.; Kurihara, H.; Yamamoto, H. *J. Org. Chem.* **1997**, *62*, S664–S665. (c) Mori, Y.; Manabe, K.; Kobayashi, S. *Angew. Chem., Int. Ed.* **2001**, *40*, 2815–2818. (d) Tanaka, Y.; Hasui, T.; Sugimoto, M. *Synlett* **2008**, 2008, 1239–1242. (e) Oishi, S.; Saito, S. *Angew. Chem., Int. Ed.* **2012**, *51*, 5395–5399. (f) El Dine, T. M.; Rouden, J.; Blanchet, J. *Chem. Commun.* **2015**, *51*, 16084–16087.
- (9) Dimitrijević, E.; Taylor, M. S. *ACS Catal.* **2013**, *3*, 945–962.
- (10) (a) Blackmond, D. G. *Angew. Chem., Int. Ed.* **2005**, *44*, 4302–4320. (b) Blackmond, D. G. *J. Am. Chem. Soc.* **2015**, *137*, 10852–10866.
- (11) (a) Lee, D.; Taylor, M. S. *J. Am. Chem. Soc.* **2011**, *133*, 3724–3727. (b) Taylor, M. S. *Acc. Chem. Res.* **2015**, *48*, 295–305.
- (12) Lee, D.; Williamson, C. L.; Chan, L.; Taylor, M. S. *J. Am. Chem. Soc.* **2012**, *134*, 8260–8267.
- (13) Chudzinski, M. G.; Chi, Y.; Taylor, M. S. *Aust. J. Chem.* **2011**, *64*, 1466–1469.
- (14) Kevill, D. N.; Daum, P. H.; Sapre, R. J. *Chem. Soc., Perkin Trans. 2* **1975**, 963–965.

- (15) Infante, I.; Bonini, C.; Lelj, F.; Righi, G. *J. Org. Chem.* **2003**, *68*, 3773–3780.
- (16) Kirby, A. J. *Stereoelectronic Effects*; Oxford Science Publications: New York, 1996.
- (17) Behrens, C. H.; Sharpless, K. B. *J. Org. Chem.* **1985**, *50*, 5696–5704.
- (18) Fox, J. M.; Dmitrenko, O.; Liao, L.-a.; Bach, R. D. *J. Org. Chem.* **2004**, *69*, 7317–7328.
- (19) Ruff, F.; Farkas, Ö. *J. Phys. Org. Chem.* **2011**, *24*, 480–491.
- (20) Williams, A. *Acc. Chem. Res.* **1989**, *22*, 387–392.
- (21) (a) Bentley, T. W.; Carter, G. E.; Harris, H. C. *J. Chem. Soc., Chem. Commun.* **1984**, 387–389. (b) Bentley, T. W.; Carter, G. E.; Harris, H. C. *J. Chem. Soc., Perkin Trans. 2* **1985**, 983–990.
- (22) Kevill, D. N.; Kim, C.-B. *J. Chem. Soc., Perkin Trans. 2* **1988**, 1353–1358.
- (23) (a) Asubiojo, O.; Brauman, J. I. *J. Am. Chem. Soc.* **1979**, *101*, 3715–3724. (b) Han, C.-C.; Brauman, J. I. *J. Am. Chem. Soc.* **1987**, *109*, 589–590.
- (24) Mello, R.; Alcalde-Aragonés, A.; Olmos, A.; González-Núñez, M. E.; Asensio, G. *J. Org. Chem.* **2012**, *77*, 4706–4710.
- (25) Lee, D.; Newman, S. G.; Taylor, M. S. *Org. Lett.* **2009**, *11*, 5486–5489.
- (26) Frisch, M. J.; Trucks, G. W.; Schlegel, H. B.; Scuseria, G. E.; Robb, M. A.; Cheeseman, J. R.; Scalmani, G.; Barone, V.; Mennucci, B.; Petersson, G. A.; Nakatsuji, H.; Caricato, M.; Li, X.; Hratchian, H. P.; Izmaylov, A. F.; Bloino, J.; Zheng, G.; Sonnenberg, J. L.; Hada, M.; Ehara, M.; Toyota, K.; Fukuda, R.; Hasegawa, J.; Ishida, M.; Nakajima, T.; Honda, Y.; Kitao, O.; Nakai, H.; Vreven, T.; Montgomery, J. A., Jr.; Peralta, J. E.; Ogliaro, F.; Bearpark, M. J.; Heyd, J.; Brothers, E. N.; Kudin, K. N.; Staroverov, V. N.; Kobayashi, R.; Normand, J.; Raghavachari, K.; Rendell, A. P.; Burant, J. C.; Iyengar, S. S.; Tomasi, J.; Cossi, M.; Rega, N.; Millam, N. J.; Klene, M.; Knox, J. E.; Cross, J. B.; Bakken, V.; Adamo, C.; Jaramillo, J.; Gomperts, R.; Stratmann, R. E.; Yazyev, O.; Austin, A. J.; Cammi, R.; Pomelli, C.; Ochterski, J. W.; Martin, R. L.; Morokuma, K.; Zakrzewski, V. G.; Voth, G. A.; Salvador, P.; Dannenberg, J. J.; Dapprich, S.; Daniels, A. D.; Farkas, Ö.; Foresman, J. B.; Ortiz, J. V.; Cioslowski, J.; Fox, D. J. *Gaussian 09*; Gaussian, Inc.: Wallingford, CT, 2009.
- (27) Becke, A. D. *J. Chem. Phys.* **1993**, *98*, 5648–5652.